

DISCRETE p -DENSITY AND COMPRESSION RADII OF LATTICE KNOTS

MAKOTO OZAWA

ABSTRACT. We introduce a framework for discrete p -density and compression-radius profiles for lattice knots. The construction is designed as a computable counterpart of ropelength-windowed geometric invariants of knot types, but the emphasis of this paper is foundational: the main output is a finite-state formalism, not a completed large-scale numerical survey. At a lattice length level N , one considers lattice-polygon representatives of a fixed knot type with length at most N , modulo lattice isometries, and optionally restricts to a seed-generated subgraph under a chosen local move system such as BFACF moves. Geometric functionals are then attached to the vertices of the filtered move graph.

To reduce lattice artefacts, the framework also permits a controlled small perturbation and corner smoothing of each lattice polygon, followed by thickness normalization. We give a concrete circular corner-rounding scheme and formulate an interval-based thickness-certification pipeline for the resulting line-and-arc curves. The smoothed profiles are therefore specified as reproducible finite computations once a certificate routine is implemented. The numerical data reported here are deliberately labelled as raw-lattice preliminary sanity checks, not as completed smoothed profiles or exhaustive BFACF sampling.

The theoretical part separates unconditional finite-state statements from open approximation questions. The finite-computability and monotonicity results are elementary finite-state bookkeeping statements, but they are recorded explicitly to make clear what a reported computation certifies. We also prove a component-profile inequality relating density minima to merge structure in the filtered move graph. As initial numerical checks, we include raw-lattice computations for the square unknot, a 24-step cubic-lattice trefoil, and a first length-filtration profile for the trefoil at levels $N = 24, 26, 28, 30, 32$ using positive plaquette detours from the seed. These data are used not as a claim of exhaustive optimization, but as evidence for a qualitative distinction: density profiles decrease toward degenerate unwindowed limits as the length cap grows, whereas compression-radius profiles optimize compactness and tend to stabilize. We also evaluate the raw density and compression values along an explicit $N = 32$ BFACF merge certificate for a figure-eight seed and its reflected mirror seed, illustrating how a merge path can temporarily worsen density while passing through compactness-improving intermediate states. A future smoothed-experiment protocol is stated for the unknot, 3_1 , 4_1 , 5_1 , 5_2 , 6_1 , 6_2 , 6_3 , 7_1 , 7_2 , the granny knot $3_1\#3_1$, and the square knot $3_1\#3_1$.

1. INTRODUCTION

This paper develops a discrete, computable model for geometric density and compression invariants of knot types. The continuous p -density and ropelength-windowed density theory is developed in [16], while the general density–compression-radius factorization for scale-covariant size functionals is developed in [17]. The starting point here is the continuous scale-free density

$$\rho_p(\gamma) = \frac{\text{Len}(\gamma)}{D_p(\gamma)},$$

where D_p is an L^p -type mean chord spread, and the compression radius

$$\text{CRad}_D(\gamma) = \frac{D(\gamma)}{\text{Thi}(\gamma)}$$

associated to a Euclidean size functional D . These quantities are invariant under similarity transformations of \mathbb{R}^3 . When optimized over all representatives of a knot type without geometric constraint, they may degenerate because one can hide the knot in a small local region and let the rest of the curve become long and nearly unknotted; this continuous degeneration is one

2020 *Mathematics Subject Classification*. Primary 57K10; Secondary 49Q10, 49Q20, 53A04, 52C25.

Key words and phrases. lattice knot, BFACF move, p -density, compression radius, ropelength, thickness, filtered move graph, smoothing certificate, raw lattice profile.

of the motivations for the ropelength-windowed theory in [16]. Ropelength-windowed variants prevent this degeneration by imposing thickness normalization and a length bound.

The present paper asks how these quantities can be computed experimentally from lattice knots. The model is motivated by the companion lattice-filtered move graph framework. There one studies, at each lattice length level N , a finite graph of lattice-polygon representatives of a knot type, with edges generated by a chosen local move system. Connected components and merge scales give a discrete analogue of ropelength-filtered admissible components. Here we enrich those graphs by attaching geometric functionals to vertices.

There are two levels of discretization. The first is purely lattice-theoretic: one evaluates ρ_p -type and CRad_D -type quantities directly on lattice polygons. This is finite and transparent, but it retains strong artefacts of the cubic lattice. The second is a smoothed lattice model: each lattice polygon is perturbed slightly and its corners are rounded, then the resulting $C^{1,1}$ curve is rescaled to thickness one. This is intended to give a closer experimental analogue of the continuous ropelength-windowed definitions. In the present version, however, the smoothed stage is a certified protocol rather than a source of large numerical tables.

The guiding principle is therefore

$$\begin{aligned} &\text{length filtration} + \text{local move graph} \\ &\quad + \text{small perturbation} + \text{corner smoothing} + \text{thickness normalization.} \end{aligned}$$

The resulting profiles are not claimed to be absolute invariants of the knot type unless the lattice, move system, smoothing class, and search region are specified. Instead, they are reproducible finite-state experimental invariants. This distinction is essential. A BFACF seed-generated computation gives information about the explored BFACF component, not automatically about the full space of all lattice representatives.

The paper is written to be self-contained at the level of definitions. The lattice-filtered move graph, the density functionals, and the compression functionals used below are all defined in the present text. The continuous papers [16, 17] are cited to identify the continuous invariants being discretized, but no result from them is used as an external hypothesis in the finite-state arguments below. The elementary finite-state propositions below should be read as reproducibility certificates rather than as deep existence theorems: the nontrivial analytic work in future experiments lies in embeddedness checking, thickness certification, and the control of search bias.

Main contributions.

- (1) We define lattice p -density and lattice compression-radius profiles on filtered lattice-polygon sets and on seed-generated move graphs.
- (2) We define smoothed-perturbed lattice profiles, obtained by replacing each lattice polygon by a controlled finite family of smoothed thickness-normalized curves; the present numerical tables are raw-lattice sanity checks, while the smoothed profiles are specified as a reproducible next experimental stage.
- (3) We record finite-state computability for fixed length level and finite smoothing scheme, and monotonicity under increasing length level; these are intentionally elementary book-keeping results that specify precisely what a finite search certifies.
- (4) We give an explicit deterministic corner-rounding scheme and outline a conservative interval-arithmetic certificate for lower-bounding thickness of the resulting line-and-arc curves.
- (5) We include pilot raw-lattice computations for the square unknot and for a trefoil seed, together with a first N -increasing raw-lattice profile for 3_1 at levels 24, 26, 28, 30, 32.
- (6) We evaluate raw density and compression-radius values along an explicit $N = 32$ BFACF merge certificate for a 30-edge figure-eight seed and its reflected mirror seed, connecting this paper's geometric profiles with the companion merge-scale computation.
- (7) We record the expected qualitative large- N behavior suggested by these profiles: un-windowed density tends toward degenerate long-loop values, while compression radius behaves as a compactness objective and is expected to stabilize at a finite positive value.

- (8) We formulate the discrete-to-continuous limit only as an open problem with scaled length windows, rather than as a claimed theorem.
- (9) We relate componentwise density and compression minima to merge structure in filtered move graphs.

Notation guide. For reference we collect the main decorated symbols used in the paper.

symbol	meaning
\mathcal{L}	a periodic lattice; in computations $\text{SC} = \mathbb{Z}^3$
$\mathcal{P}_N^{\mathcal{L}}(K)$	lattice polygons of type K with $\ell(P) \leq N$, modulo oriented lattice isometry
$G_N^{\mathcal{L}, \mathcal{M}}(K; S)$	seed-generated length- N move graph from seeds S
D_p	mean chord spread; $D_\infty = \text{diam}$
ρ_p	scale-free density Len/D_p or ℓ/D_p in the raw lattice model
CRad_D	compression radius D/Thi ; in raw SC tables $\text{Thi}_{\text{poly}} = 1/2$ is a labelled convention
$\mathcal{S}(P)$	finite smoothing/perturbation family attached to P
$\rho_{p,N}^{\mathcal{L}}, \text{CRad}_{D,N}^{\mathcal{L}}$	raw lattice level- N profiles
$\rho_{p,N}^{\mathcal{L}, \mathcal{M}, S, \text{seed}}$	seed-generated smoothed level- N profile
$\rho_{p,\lambda}^{\text{rop}}, \text{CRad}_{D,\lambda}^{\text{rop}}$	continuous ropelength-windowed profiles

2. CONTINUOUS DENSITY AND COMPRESSION FUNCTIONALS

Let γ be a tame embedded closed curve in \mathbb{R}^3 , parameterized by arclength. Write $L = \text{Len}(\gamma)$. The definitions in this section are the continuous quantities that the present lattice construction discretizes; see [16] for the p -density family and ropelength windows, and [17] for compression radii associated with general scale-covariant size functionals.

Definition 2.1 (p -spread). For $-1 < p < \infty$, $p \neq 0$, define

$$D_p(\gamma) = \left(\frac{1}{L^2} \int_\gamma \int_\gamma |x - y|^p ds_x ds_y \right)^{1/p}.$$

For $p = 0$, define $D_0(\gamma)$ by the logarithmic mean

$$\log D_0(\gamma) = \frac{1}{L^2} \int_\gamma \int_\gamma \log |x - y| ds_x ds_y,$$

whenever the integral is finite. For $p = \infty$, set

$$D_\infty(\gamma) = \text{diam}(\gamma).$$

Remark 2.2 (Why $p > -1$). The lower bound $p > -1$ is the local integrability threshold along the diagonal. Indeed, near a regular point of an embedded arclength-parametrized curve one has $|\gamma(s) - \gamma(t)| \sim |s - t|$, so the diagonal contribution is locally of the form

$$\int \int |s - t|^p ds dt,$$

which is finite precisely for $p > -1$. For $p = 0$, the logarithmic singularity is also locally integrable. In particular, for a compact embedded C^1 curve, the logarithmic mean is finite; polygonal representatives are handled edgewise, with the same local integrability at points on the same edge.

Definition 2.3 (p -density). The p -density of a representative γ is

$$\rho_p(\gamma) = \frac{\text{Len}(\gamma)}{D_p(\gamma)}.$$

Let D be a Euclidean-invariant size functional on embedded curves, homogeneous of degree one:

$$D(a\gamma) = aD(\gamma), \quad a > 0.$$

Examples include diam , the minimal enclosing radius, the radius of gyration, and D_p .

Definition 2.4 (Compression radius). The D -compression radius of γ is

$$\text{CRad}_D(\gamma) = \frac{D(\gamma)}{\text{Thi}(\gamma)}.$$

If $D = D_p$, we write $\text{CRad}_p(\gamma) = D_p(\gamma)/\text{Thi}(\gamma)$.

Lemma 2.5 (Scale invariance). For every $a > 0$,

$$\rho_p(a\gamma) = \rho_p(\gamma), \quad \text{CRad}_D(a\gamma) = \text{CRad}_D(\gamma).$$

Proof. Both Len and D_p scale by a . Similarly, both D and Thi scale by a . The ratios are therefore unchanged. \square

Definition 2.6 (Ropelength-windowed continuous profiles). Let K be a knot type and $\lambda \geq 1$. Define

$$\rho_{p,\lambda}^{\text{rop}}(K) = \inf \left\{ \frac{\text{Len}(\gamma)}{D_p(\gamma)} \mid \gamma \in K, \text{Thi}(\gamma) \geq 1, \text{Len}(\gamma) \leq \lambda \text{Rop}(K) \right\}.$$

Likewise,

$$\text{CRad}_{D,\lambda}^{\text{rop}}(K) = \inf \left\{ \frac{D(\gamma)}{\text{Thi}(\gamma)} \mid \gamma \in K, \text{Thi}(\gamma) > 0, \frac{\text{Len}(\gamma)}{\text{Thi}(\gamma)} \leq \lambda \text{Rop}(K) \right\}.$$

Remark 2.7 (Equivalent normalizations). The two displayed windows use slightly different normalizations only for notational convenience. Since ρ_p and CRad_D are scale invariant, a curve with $\text{Thi}(\gamma) > 0$ and

$$\text{Len}(\gamma)/\text{Thi}(\gamma) \leq \lambda \text{Rop}(K)$$

can be rescaled to thickness one without changing either functional. Conversely, under the condition $\text{Thi}(\gamma) \geq 1$ and $\text{Len}(\gamma) \leq \lambda \text{Rop}(K)$, the ropelength bound $\text{Len}(\gamma)/\text{Thi}(\gamma) \leq \lambda \text{Rop}(K)$ is automatic. Thus both formulations represent the same ropelength-window principle; the distinction is only a matter of whether thickness one is imposed before or after evaluating a scale-free quantity.

The length window is essential. Without it, density-type quantities may collapse under local knotting constructions and cease to detect the knot type; the continuous version of this degeneration and the ropelength-windowed refinement are studied in [16].

3. LATTICE POLYGONS AND FILTERED MOVE GRAPHS

Let \mathcal{L} be a periodic lattice in \mathbb{R}^3 . In the computational sections we specialize to the simple cubic lattice $\text{SC} = \mathbb{Z}^3$ with unit edges.

Definition 3.1 (Lattice polygon). A lattice polygon in \mathcal{L} is an embedded closed polygonal curve whose edges are lattice edges. Its lattice length is the number of lattice edges and is denoted $\ell(P)$.

For a knot type K , write

$$\mathcal{P}_N^{\mathcal{L}}(K) = \{P \subset \mathcal{L} : P \text{ is a lattice polygon of type } K, \ell(P) \leq N\} / \text{Isom}^+(\mathcal{L}).$$

Here $\text{Isom}^+(\mathcal{L})$ is the orientation-preserving lattice isometry group. If mirrors are to be identified, one may instead divide by the full lattice isometry group. In this paper mirrors are not identified unless explicitly stated.

Definition 3.2 (Lattice length minimum). The minimal lattice length of K in \mathcal{L} is

$$n_{\mathcal{L}}(K) = \min\{\ell(P) : P \subset \mathcal{L} \text{ represents } K\}.$$

Let \mathcal{M} be a specified local move system on lattice polygons, for example a BFACF-type move system in the simple cubic lattice; see [2, 3, 4] for the origins and knot-theoretic use of the BFACF algorithm.

Definition 3.3 (Filtered move graph). The lattice-filtered move graph at level N is the finite graph

$$G_N^{\mathcal{L}, \mathcal{M}}(K)$$

whose vertices are $\mathcal{P}_N^{\mathcal{L}}(K)$ and whose edges connect two vertices when they differ by one allowed move in \mathcal{M} .

Definition 3.4 (Seed-generated graph). Given a finite seed set $S \subset \mathcal{P}_{N_0}^{\mathcal{L}}(K)$, the seed-generated graph

$$G_N^{\mathcal{L}, \mathcal{M}}(K; S)$$

is the induced subgraph of $G_N^{\mathcal{L}, \mathcal{M}}(K)$ generated by all vertices reachable from S through \mathcal{M} -paths that remain at length at most N .

Remark 3.5. All BFACF computations are relative to the chosen BFACF implementation. They are not automatically exhaustive over all lattice polygons of type K unless an exhaustive enumeration or a separate completeness statement is supplied. In the simple-cubic BFACF setting, elementary moves change the length by 0 or ± 2 ; therefore a seed-generated search only visits length levels with the same parity as the chosen seed length.

Definition 3.6 (Admissible length levels). Given a move system \mathcal{M} and seed length N_0 , let

$$\mathcal{N}_{\mathcal{M}}(N_0) = \{N \geq N_0 : N \text{ is reachable as a length level from } N_0 \text{ under } \mathcal{M}\}.$$

For the simple-cubic BFACF searches used in the pilot computations, $\mathcal{N}_{\text{BFACF}}(N_0) = \{N_0, N_0 + 2, N_0 + 4, \dots\}$.

4. DISCRETE LATTICE DENSITY AND COMPRESSION PROFILES

The simplest discrete model evaluates the same pairwise-distance functionals on the polygonal curve P itself.

Definition 4.1 (Lattice p -density at level N). For a lattice polygon P , define

$$\rho_p^{\mathcal{L}}(P) = \frac{\ell(P)}{D_p(P)},$$

where $D_p(P)$ is computed using arclength measure on the polygonal curve. The level- N lattice p -density of K is

$$\rho_{p,N}^{\mathcal{L}}(K) = \min\{\rho_p^{\mathcal{L}}(P) : P \in \mathcal{P}_N^{\mathcal{L}}(K)\}.$$

For a seed set S , define

$$\rho_{p,N}^{\mathcal{L}, \mathcal{M}, \text{seed}}(K; S) = \min\{\rho_p^{\mathcal{L}}(P) : P \in G_N^{\mathcal{L}, \mathcal{M}}(K; S)\}.$$

Definition 4.2 (Lattice compression radius at level N). For a polygonal thickness $\text{Thi}_{\text{poly}}(P)$, set

$$\text{CRad}_D^{\mathcal{L}}(P) = \frac{D(P)}{\text{Thi}_{\text{poly}}(P)}.$$

Then define

$$\text{CRad}_{D,N}^{\mathcal{L}}(K) = \min\{\text{CRad}_D^{\mathcal{L}}(P) : P \in \mathcal{P}_N^{\mathcal{L}}(K)\}$$

and, for seed-generated computations,

$$\text{CRad}_{D,N}^{\mathcal{L}, \mathcal{M}, \text{seed}}(K; S) = \min\{\text{CRad}_D^{\mathcal{L}}(P) : P \in G_N^{\mathcal{L}, \mathcal{M}}(K; S)\}.$$

Proposition 4.3 (Finite-state computability). *For fixed \mathcal{L} , K , N , and finite move-generated vertex set, the quantities*

$$\rho_{p,N}^{\mathcal{L}, \mathcal{M}, \text{seed}}(K; S), \quad \text{CRad}_{D,N}^{\mathcal{L}, \mathcal{M}, \text{seed}}(K; S)$$

are finite computable real numbers up to the numerical precision used to evaluate the pairwise integrals and thickness. If $\mathcal{P}_N^{\mathcal{L}}(K)$ is explicitly enumerated, the corresponding global level- N quantities are also computable.

Proof. A seed-generated graph under a finite length cap has finitely many vertices. The functionals are evaluated on each vertex and a finite minimum is taken. The same argument applies to an exhaustive enumerated list of $\mathcal{P}_N^{\mathcal{L}}(K)$. \square

Proposition 4.4 (Monotonicity in the length level). *For $N \leq N'$ one has*

$$\rho_{p,N'}^{\mathcal{L}}(K) \leq \rho_{p,N}^{\mathcal{L}}(K), \quad \text{CRad}_{D,N'}^{\mathcal{L}}(K) \leq \text{CRad}_{D,N}^{\mathcal{L}}(K),$$

whenever both sides are defined. The same holds for seed-generated profiles provided the seed-generated vertex sets are nested with N .

Proof. The level- N feasible set is contained in the level- N' feasible set, so taking minimum over the larger set cannot increase the value. \square

Remark 4.5 (Status of the finite-state propositions). Proposition 4.3 and Proposition 4.4 are deliberately elementary. Their role is not to supply a difficult existence theorem, but to distinguish three different kinds of claims: a finite value certified on a specified explored graph, an exhaustive value certified by a complete enumeration, and an unproved statement about the full space of lattice representatives. This distinction is essential for the numerical tables below.

Remark 4.6 (Simple cubic thickness). For a unit simple-cubic lattice polygon, the polygonal-thickness scale is affected both by local corner geometry and by the global distance between non-adjacent edges. Under the standard polygonal-thickness convention, an orthogonal corner contributes the local scale $1/2$, so for a polygon with a right-angle corner the polygonal thickness is at most $1/2$; equality holds only when no non-adjacent features force a smaller half-distance. Thus non-local doubly critical distances may also be relevant. In the raw tables below we use the common simple-cubic normalization

$$\text{Thi}_{\text{poly}}(P) = 1/2, \quad \text{CRad}_D^{\text{SC}}(P) = 2D(P),$$

only as a labelled lattice convention for the displayed representatives. The smoothed model avoids building the theory on this lattice-specific convention and requires an explicit thickness certificate for each rounded representative.

5. SMOOTHED AND PERTURBED LATTICE REPRESENTATIVES

Direct lattice values are useful but still strongly lattice-dependent. To obtain quantities closer to the continuous ropelength-windowed invariants, we pass from lattice polygons to smoothed, slightly perturbed curves.

Definition 5.1 (Smoothing-perturbation scheme). A smoothing-perturbation scheme $\mathcal{S} = (\varepsilon, r, \mathcal{A})$ assigns to each lattice polygon P a nonempty finite set

$$\mathcal{S}(P) = \{\gamma_1, \dots, \gamma_m\}$$

of embedded $C^{1,1}$ closed curves satisfying:

- (i) each γ_i is ambient isotopic to P ;
- (ii) γ_i lies in an ε -tubular neighborhood of P ;
- (iii) corners of P are replaced by arcs or splines of controlled radius at least r , except where the algorithm certifies a larger local radius;
- (iv) the construction is reproducible from the finite algorithmic data \mathcal{A} .

5.1. A concrete corner-rounding scheme. We now record one deterministic smoothing scheme which can be implemented without any auxiliary choices beyond a rounding radius. Let $P = (v_0, \dots, v_{n-1})$ be an oriented unit-edge simple-cubic polygon. At a turning vertex v_i , put

$$a_i = v_i - v_{i-1}, \quad b_i = v_{i+1} - v_i,$$

where indices are taken modulo n . Thus a_i is the incoming unit direction and b_i is the outgoing unit direction. If $a_i \neq b_i$, choose $0 < r < 1/2$ and replace the two trimmed subsegments ending at

$$q_i^- = v_i - ra_i, \quad q_i^+ = v_i + rb_i$$

by the quarter-circular arc of radius r in the coordinate plane spanned by a_i and b_i , centered at

$$c_i = v_i - ra_i + rb_i.$$

The case $a_i = -b_i$, corresponding to an immediate backtracking edge, cannot occur in an embedded unit-edge lattice polygon after the usual cancellation of repeated edges. Thus the only local cases for an embedded cubic-lattice polygon are a straight vertex $a_i = b_i$, where no rounding is performed, and a right-angle vertex $a_i \perp b_i$, where the above circular replacement is used. The arc is chosen with tangent a_i at q_i^- and tangent b_i at q_i^+ . Straight vertices are left unchanged. We call the resulting curve the r -rounded representative and denote it by $\gamma_r(P)$.

A finite deterministic scheme is obtained by choosing a finite list r_1, \dots, r_s of radii and setting

$$\mathcal{S}_{\text{round}}(P) = \{\gamma_{r_j}(P) : 1 \leq j \leq s\},$$

after discarding any rounded curve that fails an embeddedness certificate. A finite perturbed scheme is obtained by first replacing selected vertices by rational displacements of size at most ε and then applying the same rounding rule. In that case each accepted curve must be accompanied by the finite perturbation record and the rounding radius used.

Proposition 5.2 (Elementary thickness certificate). *Let P be a unit simple-cubic polygon and let γ be obtained from P by a rounded perturbation lying in the δ -neighborhood of P . Suppose that all non-adjacent local pieces of the smoothing are certified to have mutual distance at least $1 - 2\delta$, and that all smoothing arcs have radius at least r . Then*

$$\text{Thi}(\gamma) \geq \min \left\{ r, \frac{1 - 2\delta}{2} \right\}.$$

Proof. For a $C^{1,1}$ curve, thickness is the minimum of the minimum radius of curvature and one half of the doubly critical self-distance. The curvature radius of each circular smoothing arc is at least r , and the straight pieces have infinite curvature radius. The assumed non-local separation gives a lower bound $1 - 2\delta$ for the relevant self-distances. Taking the minimum gives the claim. \square

Remark 5.3. The preceding proposition is intentionally conservative. Its purpose is not to produce sharp thickness values, but to ensure that every reported smoothed value can be normalized by a certified positive lower bound for thickness. The non-adjacent-distance hypothesis is a genuine global condition, not an automatic consequence of small rounding: densely packed lattice polygons may contain nearby non-adjacent strands, and then the certificate can fail unless the distance check is performed explicitly. Sharper experiments should replace this bound by interval subdivision or exact segment-arc distance calculations.

5.2. A finite thickness-certification pipeline. For the rounded representatives used here, each curve is a finite union of line segments and circular arcs. Hence a practical thickness certificate can be formulated without referring to a black-box smooth curve routine. The following procedure is the one intended for the smoothed experiments.

- (C1) Decompose γ into finitely many elementary pieces: line segments and circular arcs. Record their parameter intervals with rational or interval endpoints.
- (C2) For every adjacent pair, certify the prescribed tangent matching and record the local curvature radius. For the circular rounding scheme this lower bound is at least the chosen radius r ; for straight pieces it is infinite.
- (C3) For every non-adjacent pair of elementary pieces, compute a certified lower bound for the distance between the two parameterized pieces. This can be done by interval subdivision: on a rectangle of parameters $I \times J$, use interval arithmetic to bound the range of

$$f(s, t) = |\gamma_i(s) - \gamma_j(t)|^2.$$

If the interval lower bound is inconclusive, subdivide $I \times J$ until the required tolerance is reached.

- (C4) Take the minimum of the local radius bound and one half of the certified non-local distance bound. This gives a certified lower bound

$$\text{Thi}(\gamma) \geq \tau_{\text{cert}} > 0.$$

The value reported in numerical tables should be computed using the conservative normalization by τ_{cert} unless a sharper certified thickness value is available.

This gives a finite algorithm whenever the curve has a positive separation margin and the subdivision tolerance is fixed in advance. In implementations, one may use standard interval arithmetic packages or a bounding-volume hierarchy as an acceleration layer; these affect efficiency but not the mathematical structure of the certificate.

Proposition 5.4 (Certified computability for line-and-arc smoothing). *Fix a finite search graph, a finite list of rounding radii, and a fixed interval subdivision tolerance. Suppose each accepted rounded curve has a positive certified separation margin. Then the corresponding thickness-normalized smoothed density and compression values are reproducibly computable with a certified lower bound for thickness.*

Proof. There are finitely many curves and finitely many pairs of elementary pieces for each curve. The local curvature-radius bounds are explicit. The interval subdivision step gives finite lower bounds for all non-adjacent piece distances under the stated positive-margin hypothesis and fixed tolerance. Combining these bounds gives a positive certificate τ_{cert} , after which the density and compression quantities are evaluated by finite quadrature or by closed-form line-and-arc integrals to the prescribed accuracy. \square

Definition 5.5 (Thickness normalization). For $\gamma \in \mathcal{S}(P)$ with $\text{Thi}(\gamma) > 0$, define

$$\hat{\gamma} = \frac{1}{\text{Thi}(\gamma)}\gamma.$$

Then $\text{Thi}(\hat{\gamma}) = 1$.

Because ρ_p and CRad_D are scale invariant, the normalization is mainly a way to put the curve into the same geometric scale as ropelength theory. In particular,

$$\rho_p(\hat{\gamma}) = \rho_p(\gamma), \quad \text{CRad}_D(\hat{\gamma}) = \text{CRad}_D(\gamma).$$

Definition 5.6 (Smoothed lattice p -density). For a finite smoothing-perturbation scheme \mathcal{S} , define

$$\rho_{p,N}^{\mathcal{L},\mathcal{S}}(K) = \min \{ \rho_p(\hat{\gamma}) \mid P \in \mathcal{P}_N^{\mathcal{L}}(K), \gamma \in \mathcal{S}(P) \}.$$

For a seed set S and move system \mathcal{M} , define

$$\rho_{p,N}^{\mathcal{L},\mathcal{M},\mathcal{S},\text{seed}}(K; S) = \min \left\{ \rho_p(\hat{\gamma}) \mid P \in G_N^{\mathcal{L},\mathcal{M}}(K; S), \gamma \in \mathcal{S}(P) \right\}.$$

Definition 5.7 (Smoothed lattice compression radius). Similarly,

$$\text{CRad}_{D,N}^{\mathcal{L},\mathcal{S}}(K) = \min \{ \text{CRad}_D(\hat{\gamma}) \mid P \in \mathcal{P}_N^{\mathcal{L}}(K), \gamma \in \mathcal{S}(P) \},$$

and

$$\text{CRad}_{D,N}^{\mathcal{L},\mathcal{M},\mathcal{S},\text{seed}}(K; S) = \min \left\{ \text{CRad}_D(\hat{\gamma}) \mid P \in G_N^{\mathcal{L},\mathcal{M}}(K; S), \gamma \in \mathcal{S}(P) \right\}.$$

Theorem 5.8 (Finite computability of smoothed profiles). *Fix K , N , a finite seed-generated graph $G_N^{\mathcal{L},\mathcal{M}}(K; S)$, and a finite smoothing-perturbation scheme \mathcal{S} . Then*

$$\rho_{p,N}^{\mathcal{L},\mathcal{M},\mathcal{S},\text{seed}}(K; S), \quad \text{CRad}_{D,N}^{\mathcal{L},\mathcal{M},\mathcal{S},\text{seed}}(K; S)$$

are finite computable quantities up to numerical precision. If the full finite set $\mathcal{P}_N^{\mathcal{L}}(K)$ is enumerated, the corresponding global smoothed quantities are also computable.

Proof. The finite graph has finitely many vertices, and each vertex has finitely many smoothed representatives. Thus the feasible set is finite. Evaluating the chosen geometric functional on each element and taking a finite minimum gives the claim. \square

Remark 5.9 (Why perturbation is not cosmetic). The perturbation step is not merely a numerical trick. It separates the geometric invariant being approximated from special symmetries and angular constraints of the simple cubic lattice. A 90° corner in a lattice polygon imposes a fixed local curvature scale, while a smoothed $C^{1,1}$ perturbation allows the experiment to probe nearby continuous representatives of the same knot type.

6. LENGTH WINDOWS AND DISCRETE-TO-CONTINUOUS COMPARISON

Let $\lambda \geq 1$. The natural lattice analogue of a ropelength window is the length cap

$$N \leq \lambda n_{\mathcal{L}}(K).$$

Since N is integral and BFACF moves in the simple cubic lattice usually change length by even numbers, the effective levels are discrete.

Definition 6.1 (Windowed smoothed lattice profiles). For the full lattice profile, define

$$\rho_{p,\lambda}^{\mathcal{L},\mathcal{S}}(K) = \min_{N \in \mathbb{Z}, N \leq \lambda n_{\mathcal{L}}(K)} \rho_{p,N}^{\mathcal{L},\mathcal{S}}(K)$$

and

$$\text{CRad}_{D,\lambda}^{\mathcal{L},\mathcal{S}}(K) = \min_{N \in \mathbb{Z}, N \leq \lambda n_{\mathcal{L}}(K)} \text{CRad}_{D,N}^{\mathcal{L},\mathcal{S}}(K).$$

For a seed-generated computation from seeds of length N_0 , the minimum is taken only over admissible levels

$$N \in \mathcal{N}_{\mathcal{M}}(N_0), \quad N \leq \lambda N_0,$$

and the full level- N set is replaced by $G_N^{\mathcal{L},\mathcal{M}}(K; S)$. In the simple-cubic BFACF pilot computations this means $N = N_0, N_0 + 2, N_0 + 4, \dots$

Problem 6.2 (Thickness-controlled lattice-smoothing approximation). *Let K be a knot type and let $\lambda \geq 1$. Suppose $\mathcal{L}_h = h\mathbb{Z}^3$ is a sequence of cubic lattices with mesh $h \rightarrow 0$. Instead of using the dimensionless cap $N \leq \lambda n_{\mathcal{L}_h}(K)$, choose caps scaled to the continuous ropelength window, for example*

$$N_h(\lambda) = \left\lfloor \frac{\lambda \text{Rop}(K)}{h} \right\rfloor$$

with the parity adjustment required by the move system. Find hypotheses on smoothing schemes \mathcal{S}_h , thickness certificates, and lattice approximation under which

$$\rho_{p,N_h(\lambda)}^{\mathcal{L}_h,\mathcal{S}_h}(K) \longrightarrow \rho_{p,\lambda}^{\text{rop}}(K)$$

and similarly for CRad_D .

Remark 6.3. This is a guiding approximation problem, not a result of the present paper. The unconditional statements below concern finite computability and monotonicity at a fixed lattice and fixed search protocol. The limit problem requires independent control of lattice approximation, smoothing, thickness certificates, and optimization error.

Problem 6.4 (Effective error bounds). *Find explicit functions $E_\rho(h, N, \varepsilon, r)$ and $E_D(h, N, \varepsilon, r)$ such that smoothed lattice profiles differ from the continuous ropelength-windowed profiles by at most these errors under stated reach and thickness hypotheses.*

7. NUMERICAL EVALUATION OF THE FUNCTIONALS

This section records the computational formulas used in the experiments.

7.1. $p = 2$. For any curve γ of length L with arclength centroid

$$\bar{x} = \frac{1}{L} \int_{\gamma} x \, ds,$$

one has

$$D_2(\gamma)^2 = \frac{1}{L^2} \int_{\gamma} \int_{\gamma} |x - y|^2 \, ds_x \, ds_y = 2R_g(\gamma)^2,$$

where

$$R_g(\gamma)^2 = \frac{1}{L} \int_{\gamma} |x - \bar{x}|^2 \, ds.$$

Thus $p = 2$ is especially stable numerically.

7.2. $p = \infty$. For $p = \infty$,

$$D_{\infty}(\gamma) = \text{diam}(\gamma).$$

For a polygonal curve, the diameter is attained by vertices. For a smoothed curve, the diameter can be approximated by sufficiently fine arclength sampling, then certified by interval or subdivision bounds if needed.

7.3. **General p .** For a polygonal curve, the double integral decomposes into a sum over pairs of edges:

$$\int_P \int_P |x - y|^p \, ds_x \, ds_y = \sum_{e,f} \int_e \int_f |x - y|^p \, ds_x \, ds_y.$$

For p outside the stable closed-form range, numerical quadrature can be applied edge-pairwise. For $-1 < p < 0$, special care is needed near the diagonal pairs $e = f$ because of the integrable singularity.

7.4. **Thickness after smoothing.** The smoothed representative γ is required to be $C^{1,1}$. Its thickness is

$$\text{Thi}(\gamma) = \min\{\text{MinRad}(\gamma), \frac{1}{2} \text{dcsd}(\gamma)\},$$

where MinRad is the minimum radius of curvature and dcsd denotes doubly critical self-distance. Numerically, both quantities should be computed with certified lower bounds when the result is to be used as more than exploratory evidence.

8. PRELIMINARY NUMERICAL SANITY CHECKS

This section supplies preliminary numerical sanity checks of the definitions before the full smoothed BFACF search is run. The values in this section are *raw lattice* values: no perturbation, corner smoothing, or thickness renormalization is applied. Thus they are not yet the final smoothed profiles. They demonstrate that the functionals are directly computable on explicit lattice representatives and that increasing the length level can change the best observed density.

For a unit-edge polygon P , the $p = 2$ value was computed from

$$D_2(P)^2 = \frac{2}{\ell(P)} \int_P |x - \bar{x}|^2 \, ds, \quad \bar{x} = \frac{1}{\ell(P)} \int_P x \, ds.$$

For the polygonal segment from a to $a + d$, where $|d| = 1$, the required exact integrals are

$$\int_0^1 (a + td) \, dt = a + \frac{d}{2}, \quad \int_0^1 |a + td|^2 \, dt = |a|^2 + a \cdot d + \frac{1}{3}.$$

The diameter was computed as the maximum distance between vertices. In the raw simple-cubic rows we use the labelled lattice-thickness convention $\text{Thi}_{\text{poly}} = 1/2$, so that $\text{CRad}_D^{\text{SC}}(P) = 2D(P)$. These raw compression values are therefore convention-dependent placeholders for the later smoothed, certified-thickness computation.

The 24-step trefoil seed used below is the cubic-lattice coordinate model available from Knot-Plot [14]; Diao proved that no nontrivial simple-cubic lattice knot has fewer than 24 steps, and

that the 24-step nontrivial examples are trefoils [6, 7]. The length-26 trefoil row is obtained from this seed by replacing the edge

$$(0, 2, 1) \rightarrow (-1, 2, 1)$$

with the plaquette detour

$$(0, 2, 1) \rightarrow (0, 3, 1) \rightarrow (-1, 3, 1) \rightarrow (-1, 2, 1).$$

This is a single embedded local length-increasing detour and hence remains in the same knot type. It is not an exhaustive level-26 computation.

K	representative	ℓ	D_2^2	D_2	D_∞	ρ_2	ρ_∞
0_1	unit square	4	2/3	0.8165	1.4142	4.8990	2.8284
0_1	1×2 rectangle	6	3/2	1.2247	2.2361	4.8990	2.6833
3_1	24-step seed	24	643/144	2.1131	4.1231	11.3576	5.8209
3_1	one +2 plaquette detour	26	5359/1014	2.2989	4.8990	11.3097	5.3072

TABLE 1. Pilot raw-lattice density values. These entries are candidate values, not exhaustive minima. The length-26 row gives an upper bound for the level-26 raw-lattice profile and shows that the length filtration can lower the observed ρ_2 and ρ_∞ values.

K	representative	ℓ	$\text{CRad}_2^{\text{SC}} = 2D_2$	$\text{CRad}_\infty^{\text{SC}} = 2D_\infty$	status
0_1	unit square	4	1.6330	2.8284	exact raw value
0_1	1×2 rectangle	6	2.4495	4.4721	exact raw value
3_1	24-step seed	24	4.2262	8.2462	seed value
3_1	one +2 plaquette detour	26	4.5978	9.7980	non-exhaustive candidate

TABLE 2. Pilot raw-lattice compression-radius values under the standard $\text{Thi}_{\text{poly}} = 1/2$ convention. The one-detour row worsens the raw compression values even though it improves the displayed density values in Table 1; this illustrates that density and compactness are competing objectives. Smoothed profiles will replace these raw values by certified thickness-normalized $C^{1,1}$ values.

Remark 8.1. The density and compression objectives need not improve simultaneously. In Table 1, the length-26 detour lowers the observed ρ_2 and ρ_∞ relative to the displayed 24-step seed, while Table 2 shows that the raw compression radii increase. This supports treating density and compression as complementary profiles on the same filtered graph rather than as interchangeable measurements.

8.1. One complete smoothing sanity check: the rounded square. As a minimal check of the smoothing-normalization pipeline, take the unit square unknot and replace each corner by a quarter circle of radius $r = 1/4$. The resulting planar $C^{1,1}$ curve consists of four line segments and four circular arcs. Its length is

$$L = 4(1 - 2r) + 2\pi r = 2 + \frac{\pi}{2} \approx 3.5708.$$

For this convex rounded square, the curvature radius is r on the arcs and the opposite-side separation is larger than $2r$, so the elementary certificate gives

$$\text{Thi}(\gamma) \geq r = 1/4.$$

The following values are obtained by direct line-and-arc quadrature. They are included only to show the full pipeline “smoothing – thickness certificate – normalization – evaluation” in a completely transparent example.

example	L	τ_{cert}	D_2	D_∞	ρ_2	CRad_2
rounded square, $r = 1/4$	3.5708	0.2500	0.7800	1.2071	4.5780	3.1199

TABLE 3. A complete smoothing sanity check for the unknot. The compression value uses the certified lower bound $\tau_{\text{cert}} = 1/4$. In general this gives the conservative certified upper value D_2/τ_{cert} for the true compression radius; in this convex rounded-square example the certificate is sharp, since the actual thickness is $r = 1/4$.

This example is not intended to optimize the unknot. Its role is to demonstrate that the smoothed framework is not merely formal: for line-and-arc curves, the quantities can be evaluated after a concrete thickness certificate has been recorded.

8.2. First length-filtration profile for the trefoil. We next record a small length-filtration experiment. Starting from the same 24-step trefoil seed, we generated candidates by applying only positive BFACF-type +2 plaquette detours and retaining embedded polygons. Thus the computation below is deliberately restricted: it is neither an exhaustive BFACF cap search nor an enumeration of all trefoil lattice polygons at the indicated lengths. Its purpose is to test whether the proposed functionals exhibit a visible length-filtration effect already in a reproducible pilot search.

For each exact length level $N = 24, 26, 28, 30, 32$, Table 4 records the number of generated candidates at that exact length and the best raw values among those candidates. Table 5 records the corresponding filtered values, namely the best values among all generated candidates of length at most N .

exact length N	generated candidates	best ρ_2	best ρ_∞	min CRad_2	min CRad_∞
24	1	11.3576	5.8209	4.2262	8.2462
26	47	11.3097	5.3072	4.1827	8.2462
28	1286	10.8903	4.8742	4.1886	8.2462
30	27018	10.3115	4.5227	4.2153	8.2462
32	485184	9.7147	4.2385	4.2420	8.2462

TABLE 4. Exact-level raw-lattice pilot profile for the trefoil. Candidates are obtained from a fixed 24-step seed by positive +2 plaquette detours only. The values are therefore non-exhaustive candidate values.

cap N	cumulative	best ρ_2	best ρ_∞	best CRad_2	best CRad_∞
24	1	11.3576	5.8209	4.2262	8.2462
26	48	11.3097	5.3072	4.1827	8.2462
28	1334	10.8903	4.8742	4.1827	8.2462
30	28352	10.3115	4.5227	4.1827	8.2462
32	513536	9.7147	4.2385	4.1827	8.2462

TABLE 5. Filtered raw-lattice pilot profile for the trefoil. The entries are minima over the generated candidates with length at most N . The column “cumulative” gives the number of generated candidates with $\ell \leq N$. The monotone behavior follows from the nested feasible sets, while the numerical improvement measures the effect of increasing the length cap within this restricted search.

The density profiles improve clearly over this range. In the filtered profile, ρ_2 decreases from 11.3576 at $N = 24$ to 9.7147 at $N = 32$, and ρ_∞ decreases from 5.8209 to 4.2385. Thus the length filtration reveals representatives that are more spread out, in the sense relevant to the density functionals, than the minimal-length seed. The extension from $N = 30$ to $N = 32$

is especially useful as a stress test: the generated exact-level set grows from 27018 to 485184 candidates, but the best density values continue to improve noticeably.

The compression profiles behave differently. The best observed CRad_2 is already achieved by length 26 in this restricted search, and the best observed CRad_∞ remains the seed value through $N = 32$. The exact-level values also show that adding length does not automatically improve compression: the best exact-level CRad_2 increases mildly after $N = 26$. This is consistent with the fact that lowering density usually favors spatially larger representatives, whereas compression radius penalizes spatial size after thickness normalization. The two families of functionals therefore give complementary, rather than redundant, measurements on the same filtered move graph.

8.3. Raw profiles along the figure-eight merge certificate. We next record how the same raw density and compression quantities behave along an explicit merge certificate coming from the companion lattice-filtered move-graph computation [?]. The path connects a supplied 30-edge simple-cubic figure-eight seed ω to its reflected mirror seed $\omega!$ under the length bound $N = 32$. It has 21 states and 20 BFACF moves and passes through a 32-edge connecting state η . The seed ω reaches η in 5 BFACF moves, while the mirror seed $\omega!$ reaches the same state in 15 BFACF moves. As in the preceding raw lattice tables, we use

$$\rho_2(P) = \frac{\ell(P)}{D_2(P)}, \quad \rho_\infty(P) = \frac{\ell(P)}{\text{diam}(P)},$$

and the labelled simple-cubic convention

$$\text{CRad}_2^{\text{SC}}(P) = 2D_2(P), \quad \text{CRad}_\infty^{\text{SC}}(P) = 2 \text{diam}(P).$$

state	role	ℓ	D_2	D_∞	ρ_2	ρ_∞	$\text{CRad}_2^{\text{SC}}$	$\text{CRad}_\infty^{\text{SC}}$
s_0	seed ω	30	2.3338	4.5826	12.8545	6.5465	4.6676	9.1652
s_5	connecting state η	32	2.3532	4.5826	13.5982	6.9830	4.7065	9.1652
s_{20}	mirror seed $\omega!$	30	2.3338	4.5826	12.8545	6.5465	4.6676	9.1652

TABLE 6. Raw density and compression-radius values at the endpoints and the connecting state of the extracted $N = 32$ BFACF merge certificate for the supplied figure-eight seed and its reflected mirror seed. These are raw lattice values, not smoothed thickness-normalized values.

The connecting state has the same diameter spread as the two seeds, but a slightly larger D_2 and two additional lattice edges. Consequently, along the passage through η one has

$$\rho_2 : 12.8545 \longrightarrow 13.5982, \quad \rho_\infty : 6.5465 \longrightarrow 6.9830,$$

and

$$\text{CRad}_2^{\text{SC}} : 4.6676 \longrightarrow 4.7065, \quad \text{CRad}_\infty^{\text{SC}} : 9.1652 \longrightarrow 9.1652.$$

Thus this particular merge certificate temporarily worsens the displayed raw density values, while leaving the diameter-based compression radius unchanged at η and slightly increasing the $p = 2$ compression radius.

The full path is more informative than the three distinguished states alone. Its edge-number sequence is

$$30, 32, 32, 32, 32, 32, 32, 32, 32, 32, 32, 30, \\ 32, 32, 32, 32, 32, 32, 30, 30, 30, 30.$$

At the intermediate state s_{10} , for example, the compression values improve to

$$\text{CRad}_2^{\text{SC}} = 4.4969, \quad \text{CRad}_\infty^{\text{SC}} = 8.2462,$$

while the density values worsen to

$$\rho_2 = 13.3425, \quad \rho_\infty = 7.2761.$$

This is a concrete path-level instance of the same phenomenon seen in the trefoil pilot search: minimizing density and minimizing compression radius are competing objectives on a filtered move graph.

Raw density and compression values along the $N = 32$ merge path

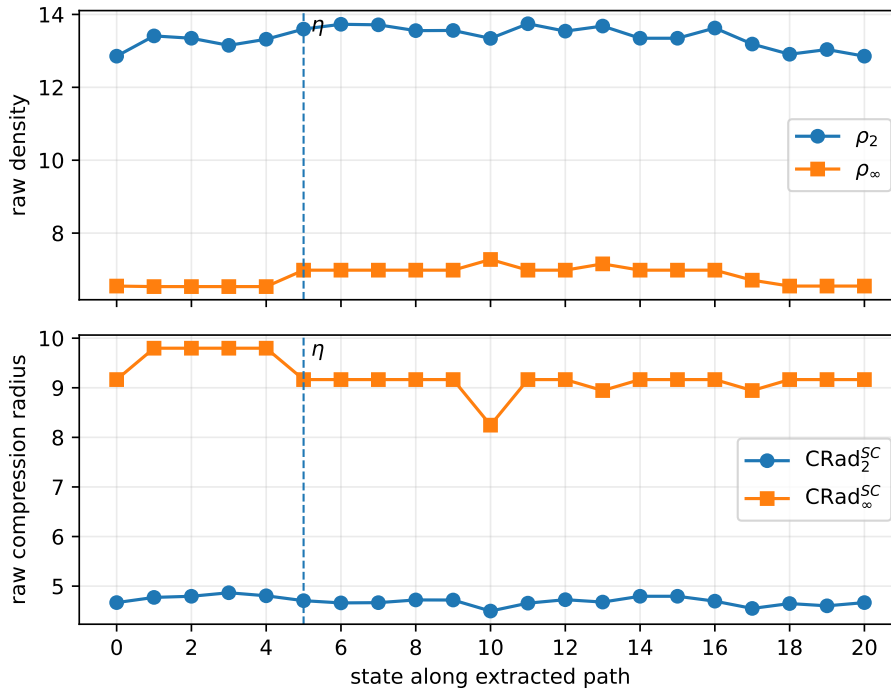


FIGURE 1. Raw density and compression values along the extracted 21-state figure-eight BFACF merge path at length bound $N = 32$. The dashed vertical line marks the connecting state $\eta = s_5$. The plotted data are raw lattice values under the labelled convention $\text{Thi}_{\text{poly}} = 1/2$.

In the raw simple-cubic convention used here, the formal product satisfies

$$\rho_D(P) \text{CRad}_D^{\text{SC}}(P) = 2\ell(P)$$

for both $D = D_2$ and $D = \text{diam}$. Hence the merge path raises the raw ropelength proxy from 60 at the 30-edge seeds to 64 at the 32-edge states and then returns to 60. This is the density–compression interpretation of the companion statement that the two seed-generated BFACF components are separated at $N = 30$ and merge at $N = 32$. The full numerical table for the 21 states is included in the supplementary data as `figure8_merge_path_density_compression.csv`.

8.4. Expected large-cap behavior and degeneracy. The filtered columns in Table 5 are monotone by construction: enlarging the length cap only enlarges the feasible set. The large- N interpretation, however, is different for density and compression. The observed behavior should not be read as convergence to a nondegenerate continuous invariant. Rather, it is evidence for why a ropelength window is needed.

This is the raw-lattice counterpart of the continuous distinction between unconstrained density degeneration [16] and compactness-type compression optimization [17].

For the diameter density,

$$\rho_\infty(P) = \frac{\ell(P)}{\text{diam}(P)},$$

there is a universal lower bound

$$\rho_\infty(P) \geq 2,$$

because any closed curve of length L has diameter at most $L/2$. Conversely, one may localize the knotted part in a bounded region and put most of the length into a long thin unknotted loop or stadium. In such a family,

$$\text{diam}(P) \sim \ell(P)/2,$$

and hence the unrestricted raw density is expected to approach the degenerate limit

$$\rho_{\infty,N}(K) \longrightarrow 2$$

as the cap tends to infinity, at least along sufficiently flexible families of lattice representatives. The trefoil values

$$5.8209, \quad 5.3072, \quad 4.8742, \quad 4.5227, \quad 4.2385$$

are consistent with the initial stage of this degeneration.

For $p = 2$ the expected limiting value depends on how much geometric freedom is allowed. In a fixed cubic lattice, a long thin out-and-back rectangular or stadium-like degeneration behaves like a doubled interval. If the doubled interval has total length L , then

$$D_2^2 \sim \frac{L^2}{24}, \quad \rho_2 \sim \sqrt{24} = 2\sqrt{6} \approx 4.8990.$$

Thus the raw cubic-lattice profile may be expected to drift toward a value near $\sqrt{24}$ in such restricted degenerating families. By contrast, if smoothing and mesh refinement allow the long unknotted part to approximate a round circle, then a circle of length L has

$$D_2 = \frac{L}{\sqrt{2\pi}}, \quad \rho_2 = \sqrt{2\pi} \approx 4.4429.$$

Accordingly, the smoothed or mesh-refined unrestricted profile may have a lower degenerate target than the fixed cubic-lattice raw profile. These values are not proposed as new knot invariants; they are benchmark degeneracies for unwidowed density.

Compression profiles have the opposite character. In the raw simple-cubic normalization used in the tables,

$$\text{CRad}_{\infty}(P) = 2 \text{diam}(P), \quad \text{CRad}_2(P) = 2D_2(P).$$

Lowering density is usually achieved by making the representative spatially larger, whereas lowering compression radius favors compact representatives. It is therefore expected that the filtered compression profiles stabilize at finite positive values associated with compact lattice representatives. In the present restricted trefoil search, the best observed value of CRad_2 is already attained at length 26, while the best observed CRad_{∞} remains the 24-step seed value throughout $N \leq 32$. A full or sampled BFACF search may lower these values, but it should not exhibit the same degeneration to the universal lower bounds seen by the density profiles.

In summary, the pilot data suggest the following qualitative picture:

quantity	observed cap behavior	expected unrestricted behavior
ρ_{∞}	decreases	degenerates toward 2
ρ_2	decreases	toward long-loop benchmarks such as $\sqrt{24}$ or $\sqrt{2\pi}$
CRad_{∞}	currently stable	finite compactness optimum
CRad_2	improves early, then stable	finite compactness optimum

This distinction is one of the main reasons for retaining the ropelength-windowed formulation in the definitions. Without such a window, the density profiles mainly detect how efficiently a knot can be hidden inside a long nearly unknotted loop; the compression profiles instead measure compactness under the chosen thickness convention or certificate.

These tables should be read as a pilot computation. In the terminology of the experimental protocol, the labels are “seed-generated”, “positive-detour restricted”, and “raw lattice”. The same table format will be used for the smoothed-thickness-normalized computations once a certified smoothing and thickness routine is incorporated. Because the number of positive-detour candidates grows rapidly, from 27018 at exact length 30 to 485184 at exact length 32, computations beyond $N = 32$ should either be explicitly labelled as larger cap searches, or else use a pruned, beam-search, or BFACF-sampling label.

9. OUTLOOK: PLANNED EXPERIMENTAL PROTOCOL FOR SMALL KNOTS

We now specify the planned computational protocol for the next experimental stage. The protocol is designed to be compatible with lattice-filtered BFACF computations and with later replacement by exhaustive minimal-layer data.

9.1. Target knot types. The first experimental set is

$$\begin{aligned} &0_1, \quad 3_1, \quad 4_1, \quad 5_1, \quad 5_2, \\ &6_1, \quad 6_2, \quad 6_3, \quad 7_1, \quad 7_2, \\ &3_1\#3_1, \quad 3_1\#\overline{3_1}. \end{aligned}$$

Here $3_1\#3_1$ is the granny knot, while $3_1\#\overline{3_1}$ denotes the square knot. We do not include a separate reflected-seed diagnostic in the present protocol, since the distance-based functionals studied here are not designed to detect chirality.

9.2. Length levels. For each knot type K , begin from one or more supplied seeds at the known or chosen birth level N_0 . Then compute at levels

$$N = N_0, N_0 + 2, N_0 + 4, \dots, N_{\max}.$$

For a window parameter λ , take

$$N_{\max} = \lfloor \lambda N_0 \rfloor$$

with parity adjusted to the move system.

K	initial length N_0	first levels	role in experiment
0_1	4	4, 6, 8, ...	calibration
3_1	24	24, 26, 28, ...	first nontrivial prime
4_1	30	30, 32, 34, ...	four-crossing prime
5_1	34	34, 36, 38, ...	torus knot test
5_2	36	36, 38, 40, ...	twist knot test
6_1	40	40, 42, 44, ...	six-crossing prime
6_2	40	40, 42, 44, ...	six-crossing prime
6_3	40	40, 42, 44, ...	six-crossing prime
7_1	44	44, 46, 48, ...	torus knot test
7_2	46	46, 48, 50, ...	seven-crossing prime
$3_1\#3_1$	40	40, 42, 44, ...	granny knot
$3_1\#\overline{3_1}$	40	40, 42, 44, ...	square knot

TABLE 7. Initial target list for length-filtered smoothed density and compression computations. The values for 0_1 and 3_1 are classical simple-cubic minimal lengths, with the trefoil minimum due to Diao [6, 7]; for the remaining small prime knots and the listed connected sums we use the standard simple-cubic minimum-length table of Janse van Rensburg and Rechnitzer [12] as the intended birth levels. In an actual data release, each seed file should still be independently checked for length, embeddedness, and knot type. If a supplied seed is not certified minimal, the corresponding N_0 should be interpreted as a supplied-seed birth level rather than a proven lattice minimum.

9.3. Per-level computation. At each level N :

- (1) Generate the reachable BFACF graph from the supplied seed set, with length cap N .
- (2) Canonicalize vertices modulo orientation-preserving lattice isometries.
- (3) For each vertex P , generate a finite family $\mathcal{S}(P)$ of smoothed perturbations.
- (4) Compute $\text{Thi}(\gamma)$, normalize to $\hat{\gamma}$, and evaluate ρ_2 , ρ_∞ , CRad_2 , and CRad_∞ .
- (5) Record the best value and the vertex/perturbation realizing it.

9.4. Output tables. The main experimental output should have one table per functional, following the format of Tables 4 and 5. For example, for ρ_2 :

K	N_0	$N_0 + 2$	$N_0 + 4$	$N_0 + 6$	best
3_1	*	*	*	*	*
4_1	*	*	*	*	*

The entries should be labelled as one of the following:

- exhaustive at level N ;
- seed-generated at level N ;
- capped search at level N ;
- stochastic perturbation search at level N .

This labelling prevents experimental values from being mistaken for absolute knot-type invariants.

10. OUTLOOK: CONNECTED-SUM TESTS

Connected sums provide a useful check on whether the profiles see composite structure. The pair $3_1\#3_1$ and $3_1\#\overline{3_1}$ will be used as a standard composite test pair. Since the functionals in this paper are based on Euclidean distances, they should not be expected to detect chirality by themselves. The point of the comparison is instead to ask how density and compression profiles behave under connected sum and whether low-density representatives emerge only after the length cap is increased.

For each composite seed, the output should report the same labels as in the prime case: whether the computation is exhaustive, seed-generated, capped, or stochastic. Any comparison between the granny and square knots must be read with this search label in mind.

11. COMPONENT PROFILES AND MERGE SCALES

The lattice-filtered move graph carries more information than a single global minimum. At level N , let \mathcal{C}_N be the set of connected components of $G_N^{\mathcal{L},\mathcal{M}}(K;S)$. For $C \in \mathcal{C}_N$, define the componentwise smoothed profile

$$\rho_p(C) = \min\{\rho_p(\hat{\gamma}) : P \in C, \gamma \in \mathcal{S}(P)\},$$

and similarly

$$\text{CRad}_D(C) = \min\{\text{CRad}_D(\hat{\gamma}) : P \in C, \gamma \in \mathcal{S}(P)\}.$$

The global seed-generated value is the minimum over components:

$$\rho_{p,N}^{\mathcal{L},\mathcal{M},\mathcal{S},\text{seed}}(K;S) = \min_{C \in \mathcal{C}_N} \rho_p(C).$$

Theorem 11.1 (Component monotonicity under merge). *Assume the seed-generated graphs are nested as N increases. Let C_1, \dots, C_m be components of $G_N^{\mathcal{L},\mathcal{M}}(K;S)$ which lie in a single component C' of $G_{N'}^{\mathcal{L},\mathcal{M}}(K;S)$ for some $N' \geq N$. Then*

$$\rho_p(C') \leq \min_{1 \leq j \leq m} \rho_p(C_j), \quad \text{CRad}_D(C') \leq \min_{1 \leq j \leq m} \text{CRad}_D(C_j).$$

Proof. Each component C_j is contained in the larger feasible component C' at level N' . The finite set over which the minimum defining $\rho_p(C')$ is taken therefore contains the feasible sets defining the $\rho_p(C_j)$. The same argument applies to CRad_D . \square

Remark 11.2. This theorem gives a simple but useful way to combine merge-scale data with geometric optimization. A merge event may lower the best density or compression value available to a component, but it cannot force the componentwise minimum to increase. Thus one can record, for each persistent component, both its merge scale and the first level at which a prescribed density or compression threshold is achieved.

12. SUMMARY OF UNCONDITIONAL RESULTS

We collect the unconditional statements which do not depend on any unproved continuous-limit assertion or on completion of the planned smoothed numerical experiments.

Theorem 12.1 (Computable smoothed lattice profiles). *Fix a knot type K , a periodic lattice \mathcal{L} , a local move system \mathcal{M} , a finite seed set S , a length cap N , and a finite smoothing-perturbation scheme \mathcal{S} . Then the smoothed seed-generated profiles*

$$\rho_{p,N}^{\mathcal{L},\mathcal{M},\mathcal{S},\text{seed}}(K; S), \quad \text{CRad}_{D,N}^{\mathcal{L},\mathcal{M},\mathcal{S},\text{seed}}(K; S)$$

are well-defined finite computable quantities. As N increases, these profiles are nonincreasing along nested seed-generated searches.

Proof. Well-definedness and finite computability follow from Theorem 5.8. Monotonicity is the same feasible-set inclusion argument as Proposition 4.4. \square

Question 12.2 (Stabilized lattice approximation with scaled windows). *Let $\mathcal{L}_h = h\mathbb{Z}^3$ and let \mathcal{S}_h be a family of smoothing schemes whose rounding radii, perturbation sizes, and certification tolerances tend to zero with h while preserving embeddedness and isotopy type. For a fixed knot type K and window parameter $\lambda \geq 1$, take the lattice length cap*

$$N_h(\lambda) = \left\lfloor \frac{\lambda \text{Rop}(K)}{h} \right\rfloor$$

with the parity adjustment required by the move system. Under what additional thickness, approximation, and optimization hypotheses do the smoothed lattice profiles with cap $N_h(\lambda)$ converge to the corresponding ropelength-windowed continuous profiles?

13. OUTLOOK: IMPLEMENTATION NOTES AND REPRODUCIBILITY

The material in this section is an implementation plan and reproducibility specification, not an additional numerical result of the present paper. The purpose is to make clear how the raw pilot computations and the planned smoothed computations should be archived and labelled.

The following pseudocode describes the intended computation.

```

for K in target_knots:
  seeds = load_seed_set(K)
  NO = initial_length(K)
  for N in admissible_levels(NO, Nmax):
    G = explore_BFACF(seeds, max_length=N)
    best = initialize_records()
    for P in G.vertices:
      for gamma in smooth_perturbations(P, eps, radius, samples):
        thi = thickness(gamma)
        gamma_hat = scale(gamma, 1/thi)
        values = evaluate_density_and_compression(gamma_hat)
        update(best, values, P, gamma)
  write_summary(K, N, best)

```

For reproducibility, each output record should include:

- (i) knot type and seed file;
- (ii) length cap N ;
- (iii) number of vertices explored;
- (iv) number of smoothing perturbations per vertex;
- (v) random seed, if stochastic perturbations are used;
- (vi) best values and the realizing vertex identifiers;
- (vii) whether the search is exhaustive, seed-generated, or capped.

Data and code availability. The supplementary code and data for the raw-lattice pilot computations in Section 8 are archived on Zenodo [18]:

<https://doi.org/10.5281/zenodo.20419442>.

The archive contains the 24-step trefoil seed coordinates, the positive +2 plaquette-detour generation script, scripts for evaluating ρ_2 , ρ_∞ , CRad_2 , and CRad_∞ , and the summary tables for $N = 24, 26, 28, 30, 32$. The computations are raw-lattice, seed-generated, positive-detour restricted, and non-exhaustive, as described above.

14. FURTHER DIRECTIONS

Several refinements are natural.

Problem 14.1 (Certified thickness for smoothed lattice curves). *Develop a certified algorithm for lower-bounding $\text{Thi}(\gamma)$ for the specific smoothing schemes used in the experiments.*

Problem 14.2 (Exhaustive minimal-layer density tables). *For each small knot type K , enumerate the full minimal simple-cubic layer $\mathcal{P}_{\text{nsc}(K)}^{\text{SC}}(K)$ and compute the exact minimum, maximum, and distribution of ρ_2 , ρ_∞ , CRad_2 , and CRad_∞ .*

Problem 14.3 (Density profiles and merge scales). *Compare the value of the best density or compression representative in each connected component of $G_N^{\mathcal{L}, \mathcal{M}}(K)$ with the merge-scale structure of the same filtered move graph.*

APPENDIX A. COORDINATE SEED USED FOR THE TREFOIL PILOT COMPUTATION

For reproducibility, we record the 24-step simple-cubic trefoil seed used in Tables 1–5. The vertices are listed cyclically, with the final vertex joined to the first by a unit edge. The coordinate list is taken from the KnotPlot coordinate page [14]; the use of a 24-step trefoil seed is consistent with Diao’s proof that the smallest nontrivial simple-cubic lattice knots have length 24 and are trefoils [6, 7].

0: (1, -1, 1) 1: (1, 0, 1) 2: (1, 1, 1) 3: (1, 2, 1)
 4: (0, 2, 1) 5: (-1, 2, 1) 6: (-1, 1, 1) 7: (-1, 0, 1)
 8: (-1, 0, 0) 9: (0, 0, 0) 10: (1, 0, 0) 11: (2, 0, 0)
 12: (2, 0, 1) 13: (2, 0, 2) 14: (1, 0, 2) 15: (0, 0, 2)
 16: (0, 0, 1) 17: (0, 1, 1) 18: (0, 1, 0) 19: (0, 1, -1)
 20: (1, 1, -1) 21: (1, 0, -1) 22: (1, -1, -1) 23: (1, -1, 0)

Using the segment formulas in Section 8, this coordinate list gives

$$D_2^2 = \frac{643}{144}, \quad D_2 \approx 2.1131,$$

which verifies the first trefoil row of Table 1. The length-26 candidate in that table is obtained by replacing the edge from vertex 4 to vertex 5 by the detour

$$(0, 2, 1) \rightarrow (0, 3, 1) \rightarrow (-1, 3, 1) \rightarrow (-1, 2, 1).$$

DECLARATION OF GENERATIVE AI AND AI-ASSISTED TECHNOLOGIES

During the preparation of this manuscript, the author used ChatGPT (OpenAI, GPT-5.5 Thinking) for language polishing, organizational suggestions, preliminary consistency checks, and assistance in drafting some explanatory text and code comments. The mathematical definitions, statements, proofs, computations, references, code, and conclusions were checked and verified by the author, who takes full responsibility for the content of the paper.

REFERENCES

- [1] T. Ashton, J. Cantarella, M. Piatek, and E. Rawdon, *Knot tightening by constrained gradient descent*, Experiment. Math. **20** (2011), no. 1, 57–90.
- [2] B. Berg and D. Förster, *Random paths and random surfaces on a digital computer*, Phys. Lett. B **106** (1981), 323–326.
- [3] C. Aragão de Carvalho, S. Caracciolo, and J. Fröhlich, *Polymers and $g|\varphi|^4$ theory in four dimensions*, Nucl. Phys. B **215** (1983), 209–248.
- [4] E. J. Janse van Rensburg and S. G. Whittington, *The BFACF algorithm and knotted polygons*, J. Phys. A **24** (1991), 5553–5567.
- [5] J. Cantarella, R. B. Kusner, and J. M. Sullivan, *On the minimum ropelength of knots and links*, Invent. Math. **150** (2002), 257–286.
- [6] Y. Diao, *Minimal knotted polygons on the cubic lattice*, J. Knot Theory Ramifications **2** (1993), no. 4, 413–425.
- [7] Y. Diao, *The number of smallest knots on the cubic lattice*, J. Statist. Phys. **74** (1994), 1247–1254.
- [8] P. Exner, E. M. Harrell, and M. Loss, *Inequalities for means of chords, with application to isoperimetric problems*, Lett. Math. Phys. **75** (2006), 225–233.
- [9] O. Gonzalez and J. H. Maddocks, *Global curvature, thickness, and the ideal shapes of knots*, Proc. Natl. Acad. Sci. USA **96** (1999), 4769–4773.
- [10] E. J. Janse van Rensburg, *The Statistical Mechanics of Interacting Walks, Polygons, Animals and Vesicles*, Oxford University Press, 2015.
- [11] R. A. Litherland, J. Simon, O. Durumeric, and E. Rawdon, *Thickness of knots*, Topology Appl. **91** (1999), 233–244.
- [12] E. J. Janse van Rensburg and A. Rechnitzer, *Minimal knotted polygons in the cubic lattice*, J. Phys. A **44** (2011), 165001.
- [13] J. O’Hara, *Energy of a knot*, Topology **30** (1991), 241–247.
- [14] R. Scharein, *KnotPlot cubic-lattice knot coordinates*, KnotPlot data page, available at <https://knotplot.com/EquiLat/coords.html> (accessed for the coordinate seed recorded in Appendix A).
- [15] M. Ozawa, *Experimental Discrete Knot Theory via Lattice-Filtered Move Graphs: Seed-Generated BFACF Graphs and Merge Scales*, arXiv:2605.25322.
- [16] M. Ozawa, *Unconstrained and Ropelength-Windowed p -densities of Knot Types*, arXiv:2604.23621.
- [17] M. Ozawa, *Geometric densities and compression radii of knot types*, arXiv:2604.27912.
- [18] M. Ozawa, *Supplementary code and data for “Discrete p -Density and Compression Radii of Lattice Knots”*, Zenodo, 2026. <https://doi.org/10.5281/zenodo.20419442>.
- [19] E. J. Rawdon, *Approximating the thickness of a knot*, Ideal Knots, Ser. Knots Everything **19**, World Scientific, 1998, 143–150.
- [20] E. J. Rawdon and J. K. Simon, *Polygonal approximation and energy of smooth knots*, J. Knot Theory Ramifications **15** (2006), 429–451.

DEPARTMENT OF NATURAL SCIENCES, KOMAZAWA UNIVERSITY, TOKYO, JAPAN
 Email address: w3c@komazawa-u.ac.jp